Volume 6, Issue 1, 2016, 1070-1074 ISSN 2069-5837
Biointerface Research in Applied Chemistry
www.BiointerfaceResearch.com
Original Research Article Open Access Journal
Received: 22.01.2016 / Revised: 07.02.2016 / Accepted: 09.02.2016 / Published on-line: 14.02.2016

Facile hydrothermal synthesis of flowerlike MnO_2 constructed by ultrathin nanosheets for supercapacitors

Zhongchun Li[1,2,*], Jie Xu[1]
[1]School of Chemistry and Environmental Engineering, Jiangsu University of Technology, Changzhou, 213001, P.R. China
[2]Jiangsu Key Laboratory of Precious Metals Chemistry and Engineering, Changzhou, 213001, P.R. China
*corresponding author e-mail address: ***czlizc@126.com***

ABSTRACT
Flowerlike manganese dioxide (MnO_2) built up of ultrathin nanosheets was successfully prepared without any template or surfactant, using a facile hydrothermal route based on the redox reaction between ammonium iron (II) sulfate ($(NH_4)_2Fe(SO_4)_2·6H_2O$) and potassium permanganate ($KMnO_4$). X-ray diffraction (XRD), transmission electron microscopy (TEM) and high-resolution transmission electron microscopy (HRTEM) were used to characterize the prepared samples. Furthermore, the capacitive properties of flowerlike MnO_2 were studied by cyclic voltammetry (CV) and galvanostatic charge-discharge (GCD) measurements. The specific capacitance is 189.3 $F·g^{-1}$ for flowerlike MnO_2 at a scan rates of 2 $mV·s^{-1}$ in 1.0 $mol·L^{-1}$ Na_2SO_4. The specific capacitance of flowerlike MnO_2 electrode almost keeps immovability over 200 cycles at a current density of 3.0 $A·g^{-1}$.Thus, the flowerlike MnO_2 constructed by ultrathin nanosheets can be used as a candidate electrode material for supercapacitors.
Keywords: *synthesis, manganese dioxide, capacitance, supercapacitor*

1. INTRODUCTION
Manganese dioxide is one of the most stable manganese oxides under ambient condition, which is a promising electrode material for high-performance supercapacitors because of its excellent electrochemical properties, environmental compatibility, low cost and abundance in nature [1-3]. The size and morphology of electrode materials largely affected their electrochemical capacitive performance. Therefore, to satisfy the needs, tremendous efforts have been made to synthesize MnO_2 nanostructures with different morphologies, the methods include electrochemistry [4-6], sonochemistry [7, 8], microemulsion [9, 10], precipitation [1], reflux [11], hydrothermal methods [12, 13], thermal decomposition [14], template method [15], and sol-gel method [16]. A variety of shape-controlled MnO_2 nanostructures, such as tubes [17, 18], rods [19, 20], wires [21, 22], hollow spheres [23, 24], spindles [1], sheets [15, 25], and urchins [26] have been synthesized on a large scale. MnO_2 nanostructures were usually prepared through oxidation of Mn^{2+}, reduction of MnO_4^-, or conversion from other manganese oxides. Although great effort has been made, there is still lack of effective routes to produce high quality MnO_2 nanostructures. Therefore, it is a big challenge to develop a simple, effective and mild pathway to synthesis of MnO_2 nanostructures. Recently, porous or flowerlike micro/nanostructures have attracted increasing interest owing to their large specific surface areas and short electron/ion transport pathways. To the best of our knowledge, few reports have focused on the synthesis of MnO_2 employing transition metal ions as reducing agents and structure directing agent. Herein, we propose a facile hydrothermal route to prepare flowerlike MnO_2 built up of ultrathin nanosheets in high yield via reduction of $KMnO_4$ with $(NH_4)_2Fe(SO_4)_2·6H_2O$. The morphologies of samples could be mediated by the mass ratio of $KMnO_4/(NH_4)_2Fe(SO_4)_2·6H_2O$, reaction temperature and reaction time. The electrochemical capacitive properties of the resulting flowerlike MnO_2 were studied by CV and GCD in detail. The electrochemical performance of MnO_2could be enhanced due to short diffusion length and increased active sites. Our results showed that the flowerlike $MnO_2$is a promising electrode material for high-performance supercapacitors.

2. EXPERIMENTAL SECTION
2.1. Materials.
Isopropanol, potassium permanganate, ammonium iron (II) sulfate and ethanol were analytically pure bought from Sinopharm Chemical Reagent Co. Ltd. The water used in the experiments was distilled before use.

2.2. Synthesis of flowerlike MnO_2.
0.05 g of $(NH_4)_2Fe(SO_4)_2·6H_2O$ were firstly dissolved into 15.0 mL of distilled water. Then 0.20 g of $KMnO_4$ powder was added to the above the aqueous solution under stirring condition. The mixture was poured into a 25 ml of Teflon-lined pressure vessel after stirring vigorously, and then sealed in a stainless steel autoclave. After that, the autoclave was put into an oven and maintained at 160 °C for 6 h. After the given reaction time, autoclave was naturally cooled to room temperature. The product was gathered by centrifugation, subsequently washed with distilled water and ethanol. Finally, the sample was dried in a vacuum oven.

2.3. Characterization.

X-ray diffraction (XRD) patterns were recorded on a Bruker D8 advance diffractometer with Cu *K*α radiation (λ=0.15406 nm). Tecnai-12 transmission electron microscopy (Philips) was used to obtain the morphologies of the samples. High-resolution transmission electron microscopy (HRTEM) image was acquired on a FEI Tecnai G2 F30 S-TWIN field emission transmission electron microscopy operating at an accelerating voltage of 300 kV.

2.4. Electrochemical measurements.

The flowerlike MnO_2, acetylene black and polytetrafluorene ethylene were mixed together with a weight ratio of 80%:10%:10%. Then, a suitable amount of isopropanol was added to the mixture to form homogenous paste, which was brush-coated onto nickel foam for fabricating the working electrodes. A conventional three electrode cell was applied to conduct the electrochemical tests, in which saturated calomel electrode (SCE) and platinum foil electrode acted as the reference and counter electrodes, respectively. CV and GCD measurements were carried out in 1.0 $mol \cdot L^{-1}$ Na_2SO_4 aqueous solution on a CHI 660C electrochemical workstation (Shanghai Chenhua Instrument Co. Ltd.).

3. RESULTS SECTION

3.1. Phase and morphology of MnO_2.

XRD was applied to determine the phase and composition of the prepared samples. A representative XRD pattern of prepared MnO_2 sample is demonstrated in Figure 1.

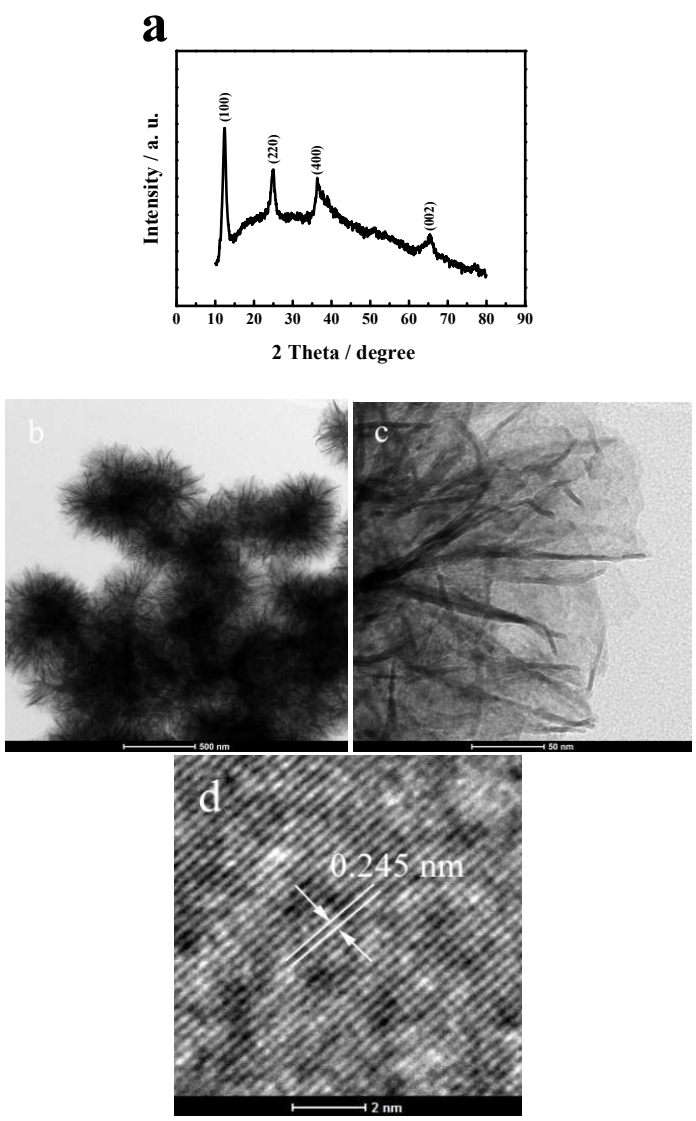

Figure 1. XRD pattern of as-prepared MnO_2 samples. (b) and (c) TEM images of MnO_2 synthesized at 160°C for 6 h with the mass ratio between $KMnO_4$ and $(NH_4)_2Fe(SO_4)_2 \cdot 6H_2O$ of 4/1. (d) HRTEM image.

Four distinct diffraction peaks are found at 2θ = 12.4°, 25.0°, 36.5°, and 65.1°, which correspond to the (110), (220), (400), and (002) reflections of tetragonal type manganese dioxide, respectively (JCPDS No. 44-0141). No obvious impurity peak was found, indicating high purity of MnO_2 obtained under the present synthetic conditions. The morphologies and microstructures of as-prepared samples were examined by TEM and HRTEM. A representative TEM image of flowerlike MnO_2 is given in Figure 1b. It is found that the sample is made up of a large quantity of flowerlike nanostructures with the size in the range of 700~1000 nm. Figure 1c displays the enlarged view of the edge of MnO_2 flowerlike architecture. From Figure 1c we can see that the flowerlike architecture is built up of many interleaving thin sheets. A structural analysis was further carried out by HRTEM. A typical HRTEM image of flowerlike MnO_2 is shown in Figure 1d. A lattice spacing of 0.245 nm shown in HRTEM image (Figure 1d) is ascribed to the (400) planes of MnO_2.

3.2. Influential factors on the formation of flowerlike MnO_2.

A series of experiments were conducted to understand the influential factors on the formation of flowerlike MnO_2. Figure 2, Figure 3 and Figure 4 show the TEM images of samples prepared under various reaction conditions.

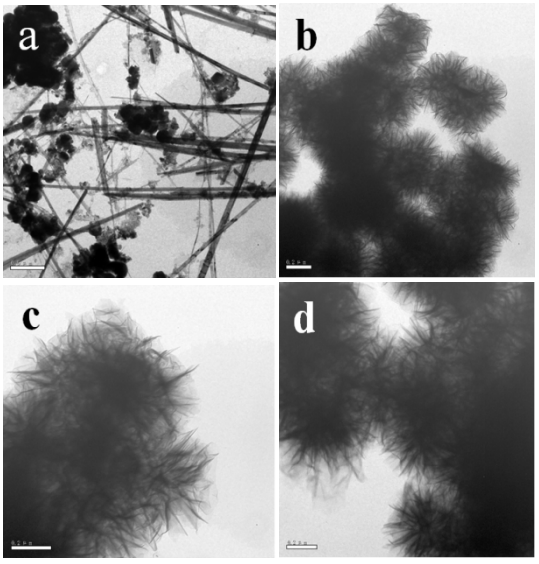

Figure 2. TEM images of samples obtained with various reaction temperatures. Reaction temperature (°C): (a) 120, (b) 140, (c) 180, (d) 200.

To investigate the effect of reaction temperature on the morphologies of samples, experiments were carried out at different temperatures (120, 140, 160, 180 and 200°C) for the same duration (6 h). Representative TEM images of samples obtained at various reaction temperatures are presented in Figure 2 and Figure 1c. When the reaction temperature was 120°C, the as-prepared sample was composed of nanowires and agglomerated nanoparticles, as shown in Figure2a. When the experiments were carried out at 140-200°C, flowerlike MnO_2 were prepared, as shown in Figure2b-d and Figure 1c.

It is found that the final morphologies of samples also depended strongly on the ratios of $KMnO_4/(NH_4)_2Fe(SO_4)_2{\cdot}6H_2O$. When the other conditions were kept constant, the morphology transformed to nanowires with the decrease of the mass ratio between $KMnO_4$ and $(NH_4)_2Fe(SO_4)_2{\cdot}6H_2O$ as depicted in Figure 3. At lower mass ratio of $KMnO_4/(NH_4)_2Fe(SO_4)_2{\cdot}6H_2O$, the concentration of Fe^{2+} is high. Fe^{2+} may preferentially bind to those facets with higher surface energy, which lead to the growth of nanowires.

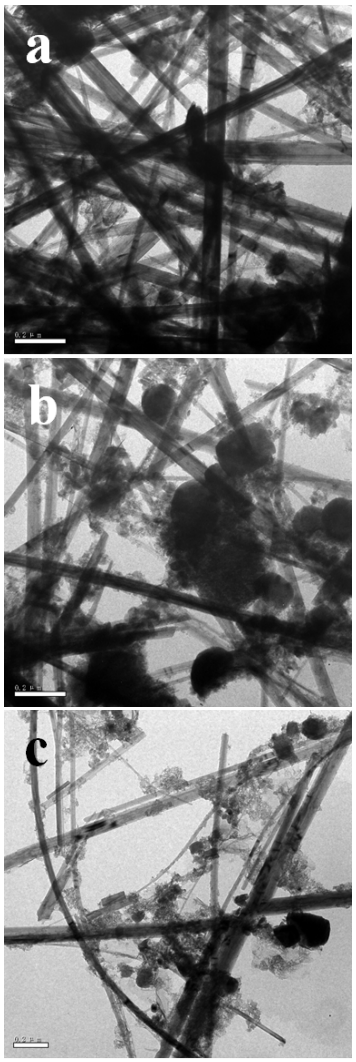

Figure 3. TEM images of samples prepared at 160°C for 6 h with various mass ratios of $KMnO_4/(NH_4)_2Fe(SO_4)_2{\cdot}6H_2O$. Mass ratios: (a) 1/1, (b) 2/3, (c) 1/2.

For clarifying the growth mechanism of flowerlike architecture, time dependent experiments were also conducted at 160°C. TEM images obtained under different hydrothermal time are shown in Figure 4. After hydrothermal reaction for 1 h, some quasi-spherical nanoparticles were formed and the surfaces of those nanoparticles were smooth (Figure 4a). When the reaction time was increased to 2 h, a few of thin layers could be found on the surfaces of the samples, as shown in shown in Figure 4b. As time goes on, the section of solid was further decreased and the size of thin sheets became larger and larger (Figure 4c). From Figure 4d we can see that the samples were entirely composed of ultrathin nanosheets when the hydrothermal time was prolonged to 6 h.

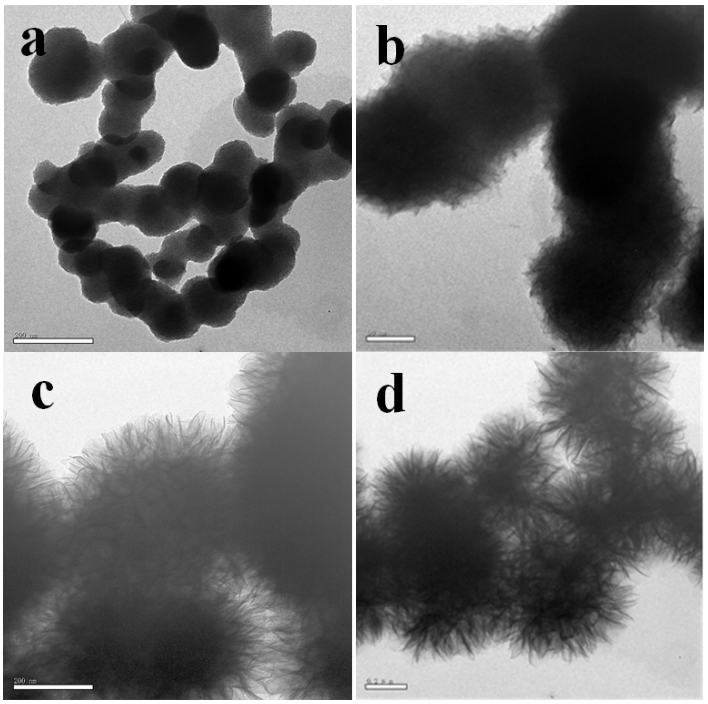

Figure 4. TEM images of samples prepared at 160°C with different reaction time. Reaction time (h): a: 1, b: 2, c: 4, d: 6.

The growth mechanism of flowerlike architecture was proposed on the base of morphology evolutions for different reaction time. The synthesis of MnO_2 is dependent on the chemical reaction between MnO_4^- and Fe^{2+}, which can be described as follows.

$$MnO_4^- + 3Fe^{2+} + 4H^+ \rightarrow MnO_2 + 3Fe^{3+} + 2H_2O$$

Firstly, the basic units of MnO_2 were formed from the redox reaction between MnO_4^- and Fe^{2+} in the solution, which would act as the nucleation seeds for the growth. In the initial stage, these units tended to aggregate to form spherical particles or quasi-spherical nanoparticles to minimize the surface energy of the initial MnO_2 units. As time goes on, MnO_2 thin layers began to grow on the surface of MnO_2 spheres, and the outmost surface of the spheres might serve as nucleation seeds. At last, the ultrathin layers grew larger and assembly to form flowerlike nanostructures.

3.3. Electrochemical performance of flowerlike MnO_2.

It is an effective way to improve the performance of electrode materials by designing electrode materials with novel microstructures. The flowerlike architecture composed of nanosheets is expected to boost the electrochemical performance of MnO_2. CV curves recorded in 1.0 $mol{\cdot}L^{-1}$ Na_2SO_4 aqueous solution at scan rates ranging from 5 to 100 $mV{\cdot}s^{-1}$ were used to elucidate the capacitive properties of flowerlike MnO_2. Typical CV curves obtained at different scan rates are shown in Figure 5.The shape of CV curves is close to rectangle, which is a fingerprint for capacitive behavior [26-28]. At higher scan rates, the shape of CV curves distorts from the rectangle, demonstrating

the larger electrical resistance of MnO_2 electrode. The specific capacitance of flowerlike MnO_2 electrode can be obtained by integrating the area of CV curve in Figure 5. The specific capacitance calculated from Figure 5 was 189.3 $F{\cdot}g^{-1}$ for flowerlike MnO_2 electrode at a scan rate of 2 $mV{\cdot}s^{-1}$. These data indicate flowerlike MnO_2 architectures possess high specific capacitance, which is more competitive than the reported values for the MnO_2 NFs and NRs (170.7 F g^{-1} and 74.7 F g^{-1}, respectively) [29]. The high specific capacitance can be attributed to great access of electrolytes to the surfaces of MnO_2nanosheets. The relation between capacitance and scan rate is shown in inset of Figure 5. The capacitance mainly arises from the insertion and release of Na^+ ions. Na^+ ions can easily diffuse into almost all available pores of the electrode at lower scan rates, leading to almost ideal capacitive behavior. The specific capacitances decrease with the increase of scan rate, which may be ascribed to the fact that Na^+ ions are not easy to enter into the pores within the MnO_2 electrode at a high scan rate, and only the outer surface of MnO_2 electrode was used to storage the charge.

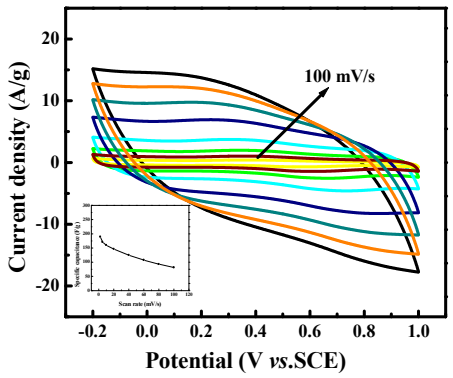

Figure 5. Cyclic voltammograms of flowerlike MnO_2. Inset: dependence of the capacitance loss on the scan rate of CV from 2 to 100 $mV{\cdot}s^{-1}$.

The galvanostatic discharge behavior of flowerlike MnO_2 was tested in 1.0 $mol{\cdot}L^{-1}$ Na_2SO_4 electrolyte at several current densities. Figure 6 shows the discharge curves of flowerlike MnO_2 at different current density.

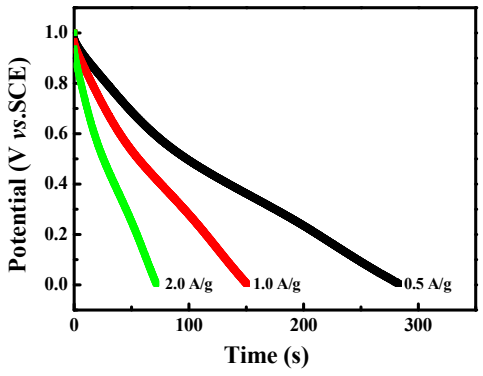

Figure 6. Discharge curves for flowerlike MnO_2 recorded at different current density.

A linear relationship between the potential and the discharge time was observed, which is another fingerprint for capacitive behavior of flowerlike MnO_2. The specific capacitance can be calculated according to $C_s=I\Delta t/\Delta Vm$ using the discharge curves. The specific capacitance is 180.5 $F{\cdot}g^{-1}$at a current density of 0.5 $A{\cdot}g^{-1}$, which is more competitive thanα-MnO_2 microspheres (124 $F{\cdot}g^{-1}$) [23], and clew-like MnO_2 (120 $F{\cdot}g^{-1}$)[26]. The results indicate that the as-prepared flowerlike MnO_2 has high specific capacitance. As we all know, high capacity is one of key factors for electrode material in practical application. Therefore, the prepared flowerlike MnO_2 has a promising application in supercapacitors.

Cycle lifetime is another important factor to evaluate a supercapacitor. The cycle performance of flowerlike MnO_2 was carried out at a current density of 3 $A{\cdot}g^{-1}$in a voltage window of 0-1.0V, as shown in Figure 7a. During the charge/discharge process, the charge curves are almost symmetric to the discharge counterparts, which indicates that flowerlike MnO_2 electrodes possess high reversibility and Coulombic efficiency. The relation between specific capacitance and cycle number is shown in Fig 7b. The specific capacitance is 169.9 $F{\cdot}g^{-1}$ for the initial cycle and retains 170.4 $F{\cdot}g^{-1}$ after 200 cycles. Such a good cycle performance may arise from the unique morphology of MnO_2. Flowerlike architectures made up of ultrathin nanosheets offer a large contact area between MnO_2 and electrolyte. The remarkable capacitive properties make the prepared flowerlike architectures to be a promising material for supercapacitors.

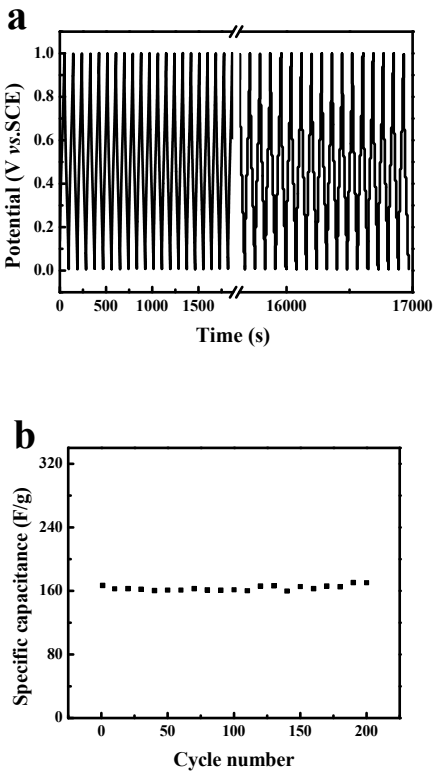

Figure 7. (a) cycling performances of flowerlike MnO_2, (b) Variation of specific capacitance versus cycle number.

4. CONCLUSIONS

In conclusion, flowerlike MnO_2 architectures were successfully prepared based on a simple hydrothermal route by reduction of $KMnO_4$ with $(NH_4)_2Fe(SO_4)_2{\cdot}6H_2O$. Flowerlike architectures were constructed by ultrathin MnO_2 nanosheets, providing a large contact area between MnO_2 and electrolyte for fast ion diffusion. When used as the electrode material for supercapacitors, flowerlike architectures exhibit high specific capacitance and good cycle stability.

5. REFERENCES

[1]Chen S., Zhu J., Han Q. ,Zheng Z., Yang Y., Wang X., Shape-controlled synthesis of one-dimensional MnO_2 via a facile quick-precipitation procedure and its electrochemical properties, *Cryst Growth Des*, 9, 10, 4356-4361, **2009.**

[2]Subramanian V., Zhu H., Wei B., Alcohol-assisted room temperature synthesis of different nanostructured manganese oxides and their pseudocapacitance properties in neutral electrolyte, *Chem Phys Lett*, 453, 4-6, 242-249, **2008.**

[3]Nakayama M., Kanaya T., Inoue R., Anodic deposition of layered manganese oxide into a colloidal crystal template for electrochemical supercapacitor, *Electrochem Commun*, 9, 5, 1154-1158, **2007.**

[4] Chang J.K., Hsu S.H., Tsai W.T., Sun I.W., A novel electrochemical process to prepare a high-porosity manganese oxide electrode with promising pseudocapacitive performance, *J Power Sources*, 177, 2, 676-680, **2008.**

[5] Chang J.K., Chen Y.L., Tsai W.T., Effect of heat treatment on material characteristics and pseudo-capacitive properties of manganese oxide prepared by anodic deposition, *J Power Sources*,135, 1-2, 344-353, **2004.**

[6]Dong B., Xue T., Xu C.L., Li H.L., Electrodeposition of mesoporous manganese dioxide films from lyotropic liquid crystalline phases, *Micropor Mesopor Mat*, 112, 1-3, 627-631, **2008.**

[7]Ghaemi M., Ataherian F., Zolfaghari A., Jafari S.M., Charge storage mechanism of sonochemically prepared MnO_2 as supercapacitor electrode: Effects of physisorbed water and proton conduction, *Electrochim Acta*, 53, 14, 4607-4614, **2008.**

[8] Kumar V.G., Kim K.B., Organized and highly dispersed growth of MnO2 nano-rods by sonochemical hydrolysis of Mn(III)acetate, *Ultrason Sonochem*, 13, 6, 549-556, **2006.**

[9]Devaraj S., Munichandraiah N., Effect of Crystallographic structure of MnO_2 on its electrochemical capacitance properties, *J Phys Chem C*, 112, 11, 4406-4417, **2008.**

[10]Yu P., Zhang X., Chen Y., Ma Y., Qi Z., Preparation and pseudo-capacitance of birnessite-type MnO_2 nanostructures via microwave-assisted emulsion method, *Mater Chem Phys*, 118, 2-3, 303-307, **2009.**

[11] Villegas J.C., Garces L.J., Gomez S., Durand J.P., Suib S.L., Particle size control of cryptomelane nanomaterials by use of H_2O_2 in acidic conditions, *Chem Mater*, 17, 7, 1910-1918, **2005.**

[12]Yan D., Yan P., Cheng S., Chen J., Zhuo R., Feng J., Zhang G., Fabrication, in-depth characterization, and formation mechanism of crystalline porous birnessite MnO_2 film with amorphous bottom layers by hydrothermal method, *Cryst Growth Des*, 9, 1, 218-222, **2008.**

[13]Subramanian V., Zhu H., Vajtai R., Ajayan P.M., Wei B., Hydrothermal synthesis and pseudocapacitance properties of MnO_2nanostructures, *J Phys Chem B*, 109, 43, 20207-20214, **2005.**

[14]Yu C., Zhang L., Shi J., Zhao J., Gao J., Yan D., A simple template-free strategy to synthesize nanoporous manganese and nickel oxides with narrow pore size distribution, and their electrochemical properties, *Adv Funct Mater*,18, 10, 1544-1554, **2008.**

[15] Fei J.B., Cui Y., Yan X.H., Qi W., Yang Y., Wang K.W., He Q., Li J.B., Controlled preparation of MnO_2hierarchical hollow nanostructures and their application in water treatment, *Adv Mater*, 20, 3, 452-456, **2008.**

[16]Wang X., Wang X., Huang W., Sebastian P.J., Gamboa S., Sol-gel template synthesis of highly ordered MnO_2 nanowire arrays, *J Power Sources*,140, 1, 211-215, **2005.**

[17] Wu M.S., Lee J.T., Wang Y.Y., Wan C.C., Field emission from manganese oxide nanotubes synthesized by cyclic voltammetric electrodeposition, *J Phys Chem B*, 108, 42, 16331-16333, **2004.**

[18]Zheng D., Sun S., Fan W., Yu H., Fan C., Cao G., Yin Z., Song X., One-step preparation of single-crystalline β-MnO_2nanotubes, *J Phys Chem B*,109, 34, 16439-16443, **2005.**

[19] Sharma R.K., Oh H.S., Shul Y.G., Kim H., Growth and characterization of carbon-supported MnO_2 nanorods for supercapacitor electrode, *Physica B: Condensed Matter*, 403, 10-11, 1763-1769, **2008.**

[20]Qu Q., Zhang P., Wang B., Chen Y., Tian S., Wu Y., Holze R., Electrochemical performance of MnO_2nanorods in neutral aqueous electrolytes as a cathode for asymmetric supercapacitors, *J Phys Chem C*, 113, 31, 14020-14027, **2009.**

[21] Xu C.L., Bao S.J., Kong L.B., Li H., Li H.L., Highly ordered MnO_2 nanowire array thin films on Ti/Si substrate as an electrode for electrochemical capacitor, *J Solid State Chem*,179, 5, 1351-1355, **2006.**

[22]Wang N., Pang H., Peng H., Li G., Chen X., Hydrothermal synthesis and electrochemical properties of MnO_2 nanostructures, *Cryst Res Technol*, 44, 11, 1230-1234, **2009.**

[23]Xu M., Kong L., Zhou W., Li H., Hydrothermal synthesis and pseudocapacitance properties of α-MnO_2 hollow spheres and hollow urchins, *J Phys Chem C*, 111, 51, 19141-19147, **2007.**

[24]Fu X., Feng J., Wang H., Ng K.M., Room temperature synthesis of a novel γ-MnO_2 hollow structure for aerobic oxidation of benzyl alcohol, *Nanotechnology*, 37, 375601, **2009.**

[25] Feng Z.P., Li G.R., Zhong J.H., Wang Z.L., Ou Y.N., Tong Y.X., MnO_2 multilayer nanosheet clusters evolved from monolayer nanosheets and their predominant electrochemical properties, *Electrochem Commun*, 11, 3, 706-710, **2009.**

[26]Yu P., Zhang X., Wang D., Wang L., Ma Y., Shape-controlled synthesis of 3D hierarchical MnO_2 nanostructures for electrochemical supercapacitors, *Cryst Growth Des*, 9, 1, 528-533, **2009.**

[27]Xiao W., Xia H., Fuh J.Y.H, Lu L., Growth of single-crystal α-MnO_2 nanotubes prepared by a hydrothermal route and their electrochemical properties, *J Power Sources*, 193, 2, 935-938, **2009.**

[28]Ragupathy P., Vasan H.N., Munichandraiah N., Synthesis and characterization of Nano-MnO_2 for electrochemical supercapacitor studies, *J Electrochem Soc*, 155, 1, A34-A40, **2008.**

[29]Li W., Liu Q., Sun Y., Sun J., Zou R., Li G., Hu X., Song G., Ma G., Yang J., Chen Z., Hu J., MnO_2 ultralong nanowires with better electrical conductivity and enhanced supercapacitor performances, *J Mater Chem*, 22, 30, 14864-14867, **2012.**

6. ACKNOWLEDGEMENTS

This work was supported by the National Natural Scientific Foundation of China (21373103). We also thank Professor Rong Guo for his help.